Science Advances
AAAS

Supplementary Materials for

Electro-mechanical coupling of KCNQ channels is a target of epilepsy-associated mutations and retigabine

Nien-Du Yang *et al.*

Corresponding author: Jianmin Cui, jcui@wustl.edu; Harley T. Kurata, kurata@ualberta.ca

Sci. Adv. **8**, eabo3625 (2022)
DOI: 10.1126/sciadv.abo3625

This PDF file includes:

Supplementary Figures

Fig. S1.

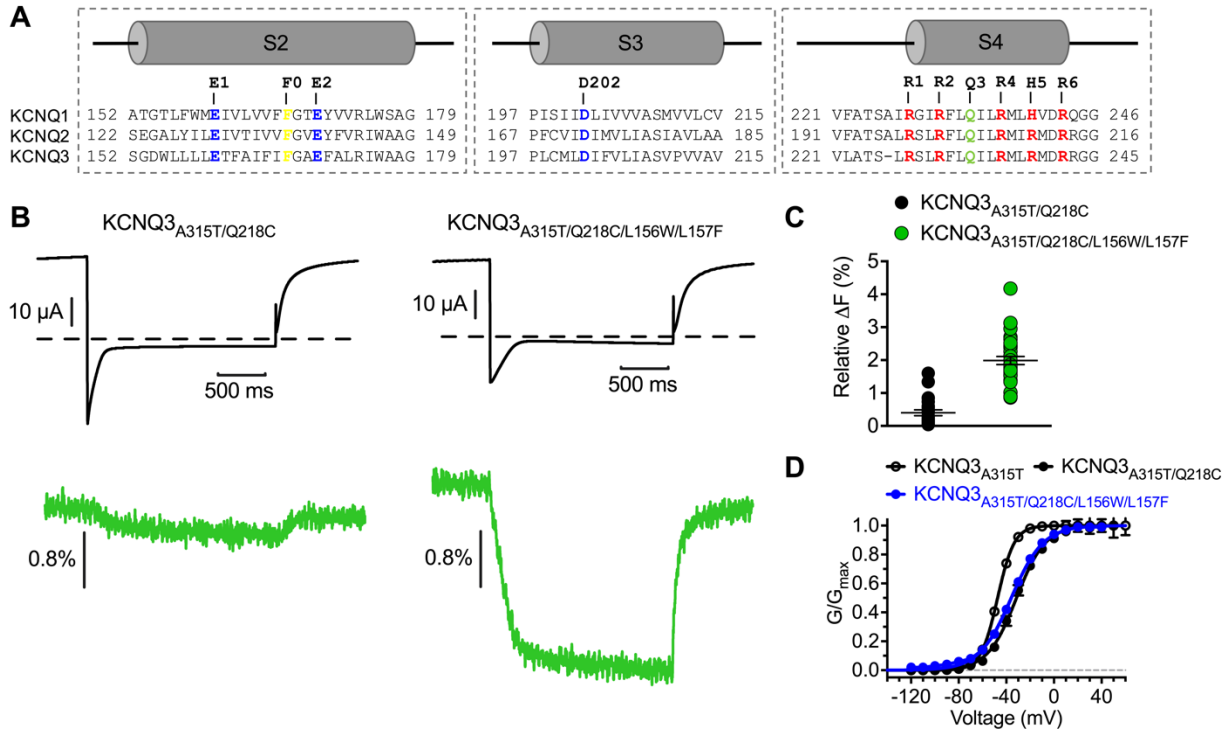

Fig. S1. Fluorescence intensity comparison and G-V relations of KCNQ3 VCF constructs. **(A)** Sequence alignment of KCNQ1-3 VSDs. R1-R6: positive gating-charges and polar residues (red and green) on S4. E1, E2, and D202: negative counter-charges (blue) on S2 and S3. F0: the aromatic "hydrophobic plug" residue (yellow) on S2. **(B)** Representative current (black) and fluorescence (green) deactivation traces for $KCNQ3_{A315T/Q218C}$ and $KCNQ3_{A315T/Q218C/L156W/L157F}$. VCF was recorded at holding potential of +40 mV, followed by a 2 s hyperpolarizing voltage pulse at -160 mV before returning to +40 mV. **(C)** Relative fluorescence signal change of $KCNQ3_{A315T/Q218C}$ (black filled circle) and $KCNQ3_{A315T/Q218C/L156W/L157F}$ (green filled circle). Circles represent individual cells recorded. **(D)** G-V relations of $KCNQ3_{A315T}$, $KCNQ3_{A315T/Q218C}$, and $KCNQ3_{A315T/Q218C/L156W/L157F}$. $V_{1/2}$ for $KCNQ3_{A315T}$ (black open circle): -47.3 ± 0.8 mV (n = 5), for $KCNQ3_{A315T/Q218C}$ (black filled circle): -31.4 ± 1.5 mV (n = 8), and for $KCNQ3_{A315T/Q218C/L156W/L157F}$ (blue filled circle): -36.0 ± 1.3 mV (n = 8).

Fig. S2.

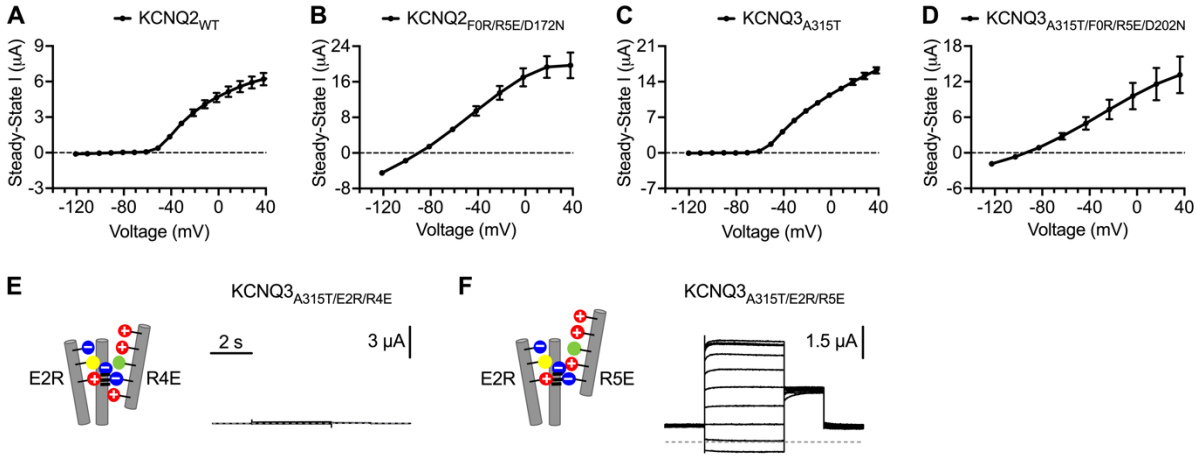

Fig. S2. Current-voltage relations of KCNQ2 and KCNQ3 double charge-reversal mutants. **(A, B)** I-V relations of $KCNQ2_{WT}$ (n = 5) and $KCNQ2_{F0R/R5E/D172N}$ (n = 5). **(C, D)** I-V relations of $KCNQ3_{A315T}$ (n = 5) and $KCNQ3_{A315T/F0R/R5E/D202N}$ (n = 5). **(E, F)** Cartoon schematics and representative current traces of additional IO-locked (E2R/R4E) and AO-locked (E2R/R5E) KCNQ3 mutant.

Fig. S3.

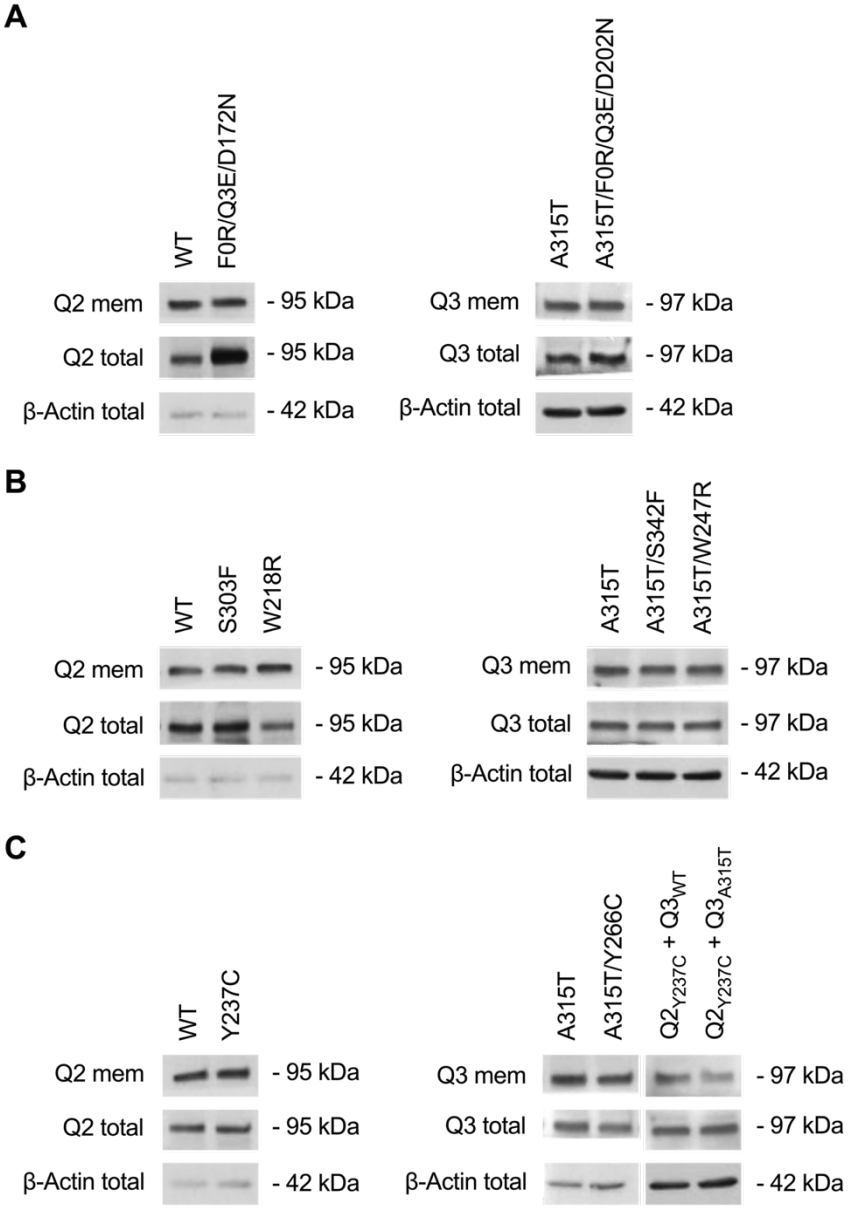

Fig. S3. Western blot results showing the membrane and total expression of various KCNQ2 and KCNQ3 mutants. Western blot probing for KCNQ2 and KCNQ3 in the membrane (top) and total (middle) fraction, and β-Actin in the total (bottom) fraction from oocytes expressing **(A)** $KCNQ2_{F0R/Q3E/D172N}$ or $KCNQ3_{A315T/F0R/Q3E/D202N}$, **(B)** $KCNQ2_{S303F}$, $KCNQ2_{W218R}$, $KCNQ3_{A315T/S342F}$, or $KCNQ3_{A315T/W247R}$, **(C)** $KCNQ2_{Y237C}$, $KCNQ2_{Y237C}$ in combination with $KCNQ3_{WT}$ or $KCNQ3_{A315T}$, or $KCNQ3_{A315T/Y266C}$. For $KCNQ2_{Y237C}$ + $KCNQ3_{WT}$ and $KCNQ2_{Y237C}$ + $KCNQ3_{A315T}$, the KCNQ3 protein was probed. $KCNQ2_{WT}$ and $KCNQ3_{A315T}$ served as positive controls. β-Actin is a cytoplasmic protein and was minimally detected in the membrane fraction of the oocytes (data not shown).

Fig. S4.

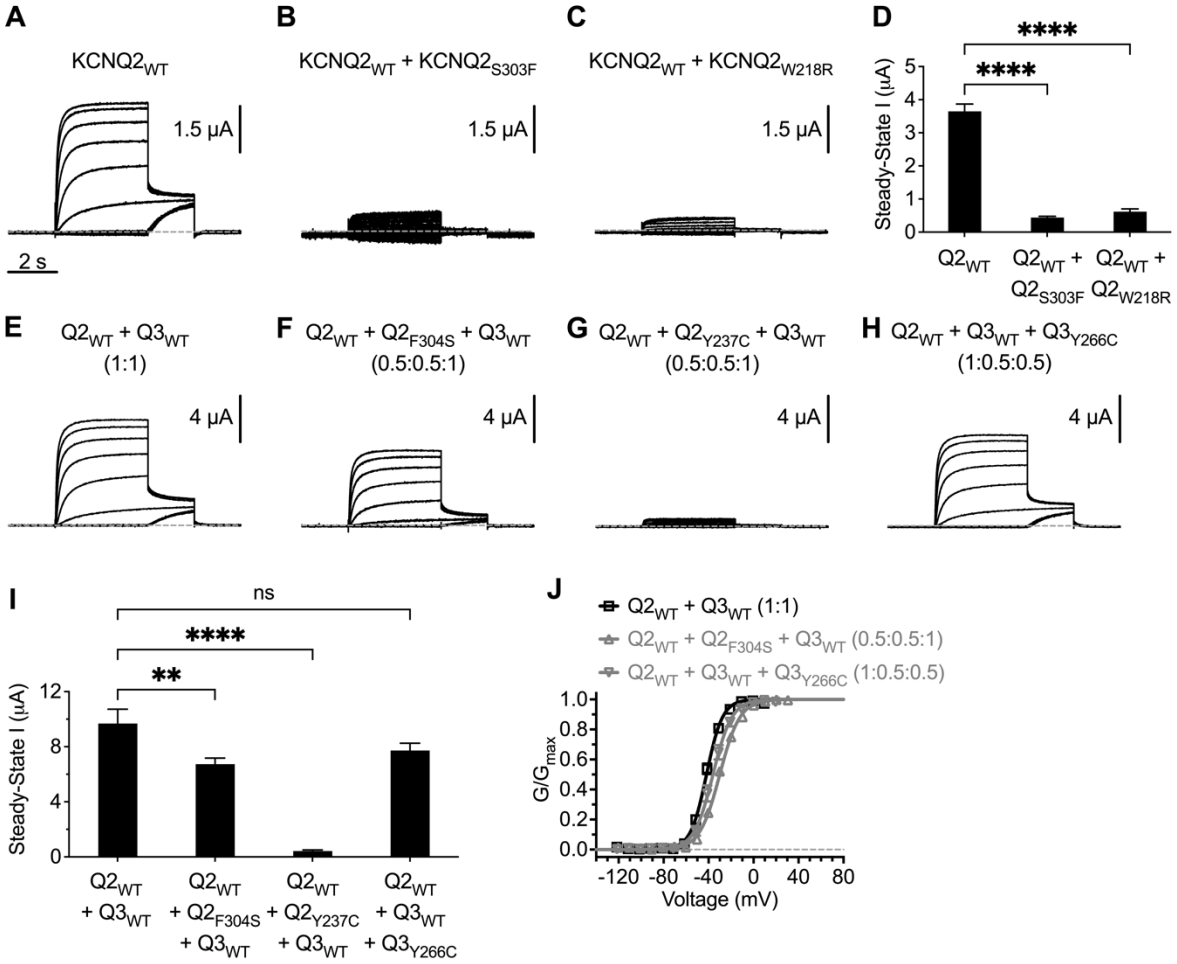

Fig. S4. Co-expression of various KCNQ2 or KCNQ3 mutants with wild-type counterparts in different ratios. (A, B, C) Representative current traces and **(D)** steady-state currents of $KCNQ2_{WT}$ with and without co-expressed $KCNQ2_{S303F}$ or $KCNQ2_{W218R}$. Current amplitudes were 3.65 ± 0.22 µA (n = 7) for $KCNQ2_{WT}$, 0.44 ± 0.04 µA (n = 5) for $KCNQ2_{S303F}$ + $KCNQ2_{WT}$ (1:1), and 0.62 ± 0.08 µA (n = 5) for $KCNQ2_{W218R}$ + $KCNQ2_{WT}$ (1:1). **(E, F, G, H)** Representative current traces, **(I)** steady-state currents, and **(J)** G-V relations of various disease-linked KCNQ2 or KCNQ3 mutants co-expressed with wild-type counterparts in different ratios. Current amplitudes were 9.68 ± 1.04 µA (n = 6) for $KCNQ2_{WT}$ + $KCNQ3_{WT}$ (1:1), 6.73 ± 0.44 µA (n = 5) for $KCNQ2_{WT}$ + $KCNQ2_{F304S}$ + $KCNQ3_{WT}$ (0.5:0.5:1), 0.42 ± 0.08 µA (n = 8) for $KCNQ2_{WT}$ + $KCNQ2_{Y237C}$ + $KCNQ3_{WT}$ (0.5:0.5:1), and 7.72 ± 0.53 µA (n = 6) for $KCNQ2_{WT}$ + $KCNQ3_{WT}$ + $KCNQ3_{Y266C}$ (1:0.5:0.5). $V_{1/2}$ for $KCNQ2_{WT}$ + $KCNQ3_{WT}$ (1:1): -41.8 ± 1.1 mV (n = 6, black open square), for $KCNQ2_{WT}$ + $KCNQ2_{F304S}$ + $KCNQ3_{WT}$ (0.5:0.5:1): -30.0 ± 0.9 mV (n = 5, gray open triangle), and for $KCNQ2_{WT}$ + $KCNQ3_{WT}$ + $KCNQ3_{Y266C}$ (1:0.5:0.5): -36.1 ± 1.9 mV (n = 6, gray open inverted triangle). Statistical significance was determined by one-way ANOVA followed by Tukey's post-hoc test. ** = $P < 0.01$. **** = $P < 0.0001$.

Fig. S5.

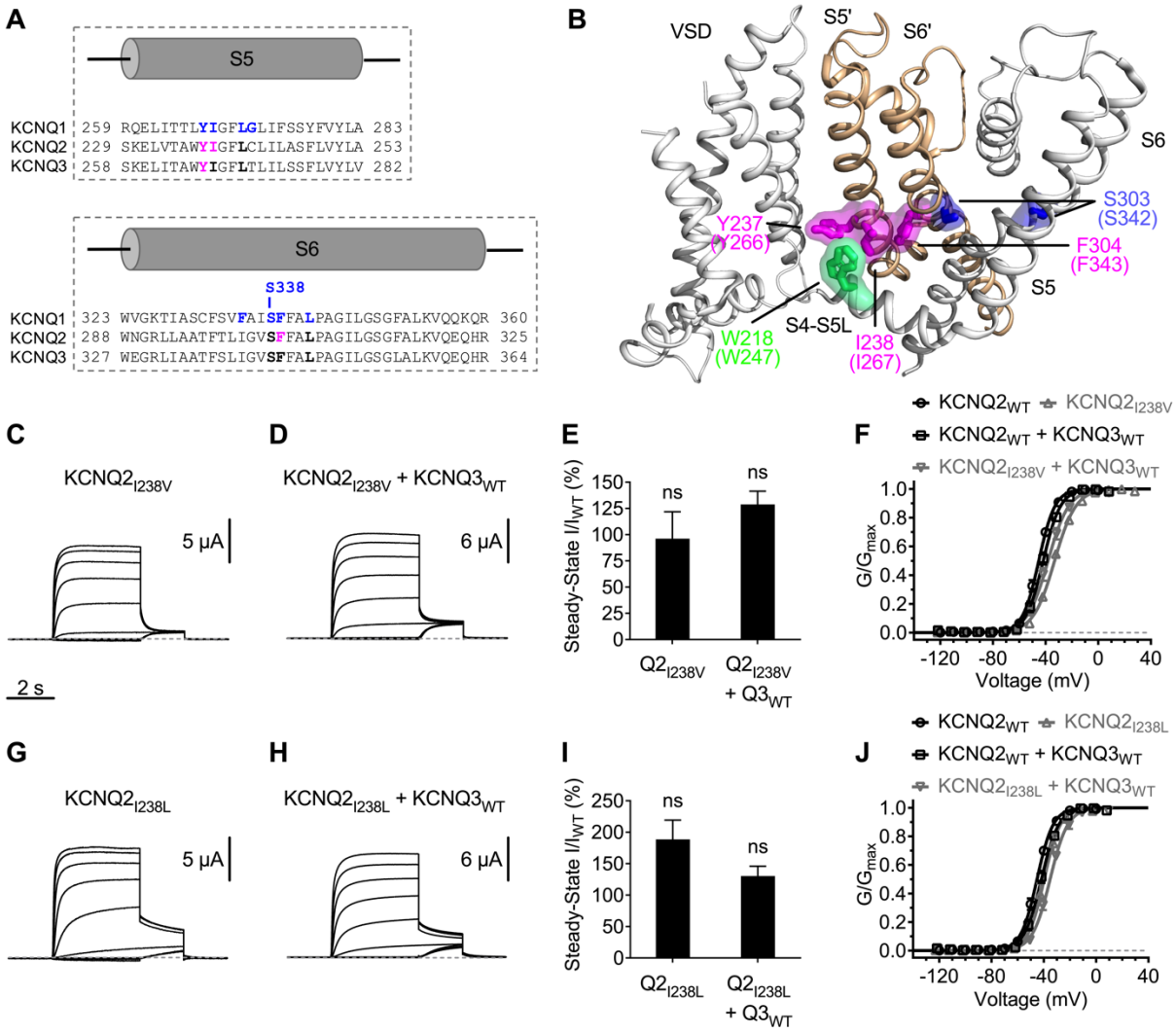

Fig. S5. The AO state E-M coupling residues in KCNQ2 and KCNQ3 associated with neonatal epilepsy and electrophysiology data of two disease-linked KCNQ2 mutants with mild effects. (A) Sequence alignment of KCNQ1-3 S5 and S6. Residues important for the KCNQ1 AO state E-M coupling are colored blue. Conserved AO state E-M coupling residues in KCNQ2 and KCNQ3 are bolded. Residues in KCNQ2 and KCNQ3 associated with neonatal epilepsy are colored magenta. **(B)** Epilepsy-linked AO state E-M coupling residues Y237, I238, and F304 (magenta) in the human KCNQ2 cryoEM structure (PDB: 7CR3). Conserved AO state E-M coupling residues W218 (green) and S303 (blue) are also shown. Brackets indicate amino acid numbers for KCNQ3. S5 and S6 from a neighboring subunit are shown in gold. **(C, D)** Representative current traces for $KCNQ2_{I238V}$ with and without co-expressed of $KCNQ3_{WT}$. **(E)** Steady-state currents normalized to $KCNQ2_{WT}$ (100 ± 24.1 %, n = 5) and KCNQ2+KCNQ3 (100 ± 4.4 %, n = 6), respectively, were 96.2 ± 25.6 % (n = 5) for $KCNQ2_{I238V}$ and 128.8 ± 12.7 % (n = 6) for $KCNQ2_{I238V}$ + $KCNQ3_{WT}$. **(F)** G-V relations of $KCNQ2_{WT}$ (black open circle), KCNQ2+KCNQ3 (black open square), $KCNQ2_{I238V}$ (gray open triangle), and $KCNQ2_{I238V}$ + $KCNQ3_{WT}$ (gray open inverted triangle). $V_{1/2}$ for $KCNQ2_{WT}$: -45.1 ± 0.9 mV (n = 5), for KCNQ2+KCNQ3: -41.8 ± 1.2 mV (n = 6), for $KCNQ2_{I238V}$: -33.1 ± 0.3 mV (n = 5), and for

$KCNQ2_{I238V}$ + $KCNQ3_{WT}$: -38.1 ± 1.5 mV (n = 9). **(G, H)** Representative current traces for $KCNQ2_{I238L}$ with and without co-expressed $KCNQ3_{WT}$. **(I)** Steady-state currents normalized to $KCNQ2_{WT}$ (100 ± 24.1 %, n = 5) and $KCNQ2_{WT}$ + $KCNQ3_{WT}$ (100 ± 4.4 %, n = 6), respectively, were 188.6 ± 30.6 % (n = 4) for $KCNQ2_{I238L}$ and 130.4 ± 15.6 % (n = 5) for $KCNQ2_{I238L}$ + $KCNQ3_{WT}$. **(J)** G-V relations of $KCNQ2_{WT}$ (black open circle), KCNQ2+KCNQ3 (black open square), $KCNQ2_{I238L}$ (gray open triangle), and $KCNQ2_{I238L}$ + $KCNQ3_{WT}$ (gray open inverted triangle). $V_{1/2}$ for $KCNQ2_{WT}$: -45.1 ± 0.9 mV (n = 5), for KCNQ2+KCNQ3: -41.8 ± 1.2 mV (n = 6), for $KCNQ2_{I238L}$: -39.7 ± 2.1 mV (n = 4), and for $KCNQ2_{I238L}$ + $KCNQ3_{WT}$: -35.1 ± 0.9 mV (n = 5). Statistical significance was determined by Student's *t* test.

Fig. S6.

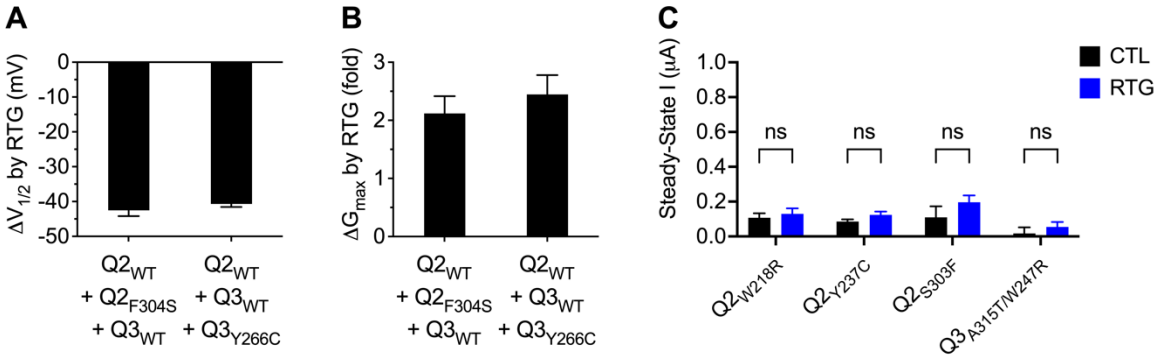

Fig. S6. Retigabine effects on KCNQ2 and KCNQ3 mutants alone and co-expressed with wild-type counterparts in different ratios. (A) Retigabine-induced shifts in $V_{1/2}$ were -42.5 ± 1.7 mV (n = 6) for $KCNQ2_{WT}$ + $KCNQ2_{F304S}$ + $KCNQ3_{WT}$ (0.5:0.5:1) and -40.7 ± 0.9 mV (n = 6) for $KCNQ2_{WT}$ + $KCNQ3_{WT}$ + $KCNQ3_{Y266C}$ (1:0.5:0.5). **(B)** Retigabine-induced increase in G_{max} (fold) were 2.12 ± 0.30 (n = 6) for $KCNQ2_{WT}$ + $KCNQ2_{F304S}$ + $KCNQ3_{WT}$ (0.5:0.5:1) and 2.45 ± 0.33 (n = 6) for $KCNQ2_{WT}$ + $KCNQ3_{WT}$ + $KCNQ3_{Y266C}$ (1:0.5:0.5). Δ G_{max} (fold) = $G_{max,RTG}/G_{max,CTL}$. **(C)** Steady-state currents of KCNQ2 and KCNQ3 mutants alone before (black) and after (blue) 100 μM retigabine. Current amplitudes in control and retigabine conditions for $KCNQ2_{W218R}$: 0.11± 0.03 μA and 0.13± 0.03 μA (n = 6), for $KCNQ2_{Y237C}$: 0.09± 0.01 μA and 0.12± 0.02 μA (n = 4), for $KCNQ2_{S303F}$: 0.11± 0.06 μA and 0.20± 0.04 μA (n = 6), and for $KCNQ3_{A315T/W247R}$: 0.02± 0.04 μA and 0.05± 0.03 μA (n = 8). Statistical significance was determined by paired Student's *t* test.

Fig. S7.

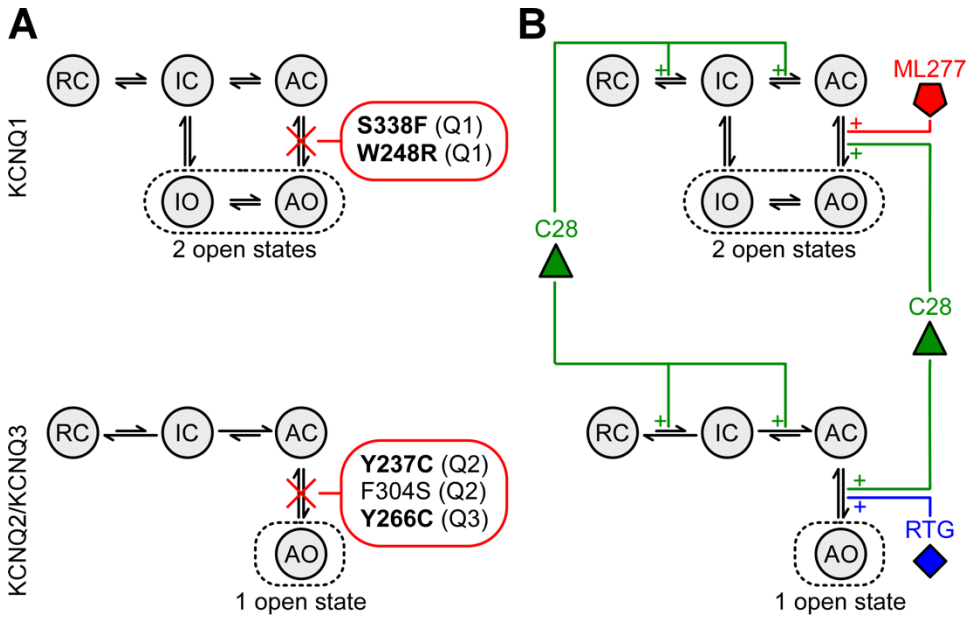

Fig. S7. Conceptual model for KCNQ channel gating, channelopathy, and pharmacology. **(A)** Gating models for KCNQ1 (top panel) and KCNQ2/KCNQ3 (bottom panel) and mechanism by which select disease-associated mutations affect the channels. For simplicity, one out of four subunits is shown. Horizontal transitions represent VSD activation and vertical transitions represent pore opening. VSD can occupy resting (R), intermediate (I), or activated (A) states. The pore can adopt closed (C) or open (O) states. The channel state is defined by a combination of VSD and pore states. State definition: Resting-Closed (RC), Intermediate-Closed (IC), Activated-Closed (AC), Intermediate-Open (IO), and Activated-Open (AO). KCNQ1 features two open states (IO and AO). By contrast, KCNQ2/KCNQ3 only conducts in the analogous AO state. Red boxes showcase select disease-associated mutations in KCNQ channels that disable AO state E-M coupling. In KCNQ1 these mutations manifest as long QT syndrome. In KCNQ2/KCNQ3 these mutations are associated with EIEE. Bolded mutations lead to complete disruption of AO state E-M coupling, while F304S partially disrupts AO state E-M coupling. **(B)** AO state E-M coupling can be pharmacologically modulated. ML277 selectively enhances AO state E-M coupling in KCNQ1, while RTG enhances AO state E-M coupling in KCNQ2/KCNQ3. C28, on the other hand, enhances AO state E-M coupling and promotes VSD activation of KCNQ1-3.

Fig. S8.

A

	Residues	References
KCNQ1 PIP2 sites	R190, R195, H258, R259, K354, K358, R360, H363, R366	(23) (61)
KCNQ3 PIP2 sites	R183, R243, K248, R371	(45)
KCNQ4 PIP2 sites	R93, R95, R159, K172, R219, R220, K225, S235, K236, H330, K333	(41)
Protein-protein sites (KCNQ2 numbering)	W218, Y237, I238, S303, F304	This study

B

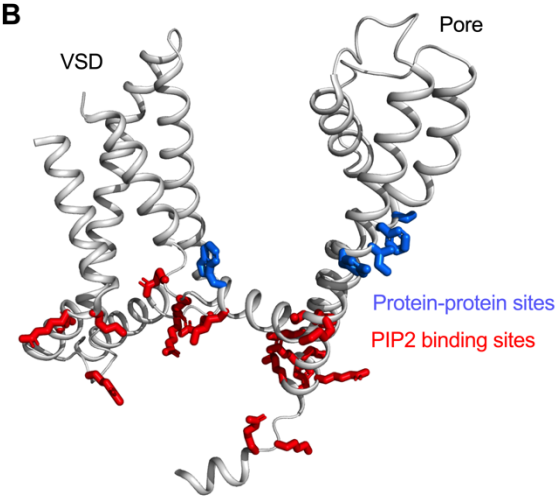

Fig. S8. Comparison of PIP2 binding sites and protein-protein E-M coupling sites in KCNQ channels. (A) Table summarizing the KCNQ PIP2 binding sites identified by previous functional and structural studies as well as the protein-protein E-M coupling sites investigated in this study. **(B)** Mapping the PIP2 binding sites (red) and the protein-protein E-M coupling sites (blue) onto the human KCNQ2 cryoEM structure (PDB: 7CR3). Colored residues are listed in table (A). Only one subunit is shown for clarity.